Evidence for Weakly Correlated Oxygen Holes in the Highest-T_c Cuprate Superconductor $HgBa_2Ca_2Cu_3O_{8+\delta}$

A. Chainani,[1,2] M. Sicot,[2] Y. Fagot-Revurat,[2] G. Vasseur,[2] J. Granet,[2] B. Kierren,[2] L. Moreau,[2] M. Oura,[1] A. Yamamoto,[3] Y. Tokura,[3] and D. Malterre[2]

[1]*RIKEN SPring-8 Centre, 1-1-1 Sayo-cho, Hyogo 679-5148, Japan*

[2]*Institut Jean Lamour, Université de Lorraine, UMR 7198 CNRS, BP70239, 54506 Vandoeuvre lés Nancy, France*

[3]*Strong Correlation Physics Division, RIKEN Center for Emergent Matter Science (CEMS), Wako 351-0198, Japan*

(Received 8 December 2016; revised manuscript received 9 May 2017; published 31 July 2017)

We study the electronic structure of $HgBa_2Ca_2Cu_3O_{8+\delta}$ (Hg1223; $T_c = 134$ K) using photoemission spectroscopy (PES) and x-ray absorption spectroscopy (XAS). Resonant valence band PES across the O K edge and Cu L edge identifies correlation satellites originating in O $2p$ and Cu $3d$ two-hole final states, respectively. Analyses using the experimental O $2p$ and Cu $3d$ partial density of states show quantitatively different on-site Coulomb energy for the Cu site ($U_{dd} = 6.5 \pm 0.5$ eV) and O site ($U_{pp} = 1.0 \pm 0.5$ eV). Cu_2O_7-cluster calculations with nonlocal screening explain the Cu $2p$ core level PES and Cu L-edge XAS spectra, confirm the U_{dd} and U_{pp} values, and provide evidence for the Zhang-Rice singlet state in Hg1223. In contrast to other hole-doped cuprates and $3d$-transition metal oxides, the present results indicate weakly correlated oxygen holes in Hg1223.

DOI: 10.1103/PhysRevLett.119.057001

Nearly 30 years after the discovery of high-transition temperature (T_c) superconductivity in the cuprates, [1] the role of electron correlations still remains the central enigma in understanding their properties. While pioneering theoretical and experimental studies have established important aspects of spin-charge ordering [2–12], antiferromagnetic correlations [13–15], and electron-phonon coupling [16] in the high-T_c cuprates, the origin for high-T_c superconductivity still remains elusive [17]. The spin-charge order competes with the metallicity of doped carriers in the CuO_2 layers and leads to novel thermodynamic, transport, and spectroscopic phenomena that favor quantum critical behavior [18–22].

It is well accepted that Mott-Hubbard correlations provide an appropriate starting point for describing the electronic structure of the CuO_2 layers [23–30]. However, the actual quantification of correlations in terms of an on-site Coulomb energy for the Cu site ($=U_{dd}$) in comparison with that on the O site ($=U_{pp}$), and their roles in spin-charge order and superconductivity, is still being investigated. In fact, using the method of Cini [31] and Sawatzky [32], as described later, it is known that U_{pp} is large (~5–6 eV) and quite comparable to U_{dd} (~5–8 eV) in $YBa_2Cu_3O_7$ [33,34], $Bi_2Sr_2CaCu_2O_8$(Bi-2212) [35], and $La_{2-x}A_xCuO_4$(A =Sr, Ba) [36]. This behavior of $U_{pp} \sim U_{dd}$ is known for oxides across the $3d$ transition metal series: titanium or vanadium oxides ($SrTiO_3$, V_2O_3, VO_2, V_2O_5) [37–39], $LaMO_3$ (M=Mn-Ni) perovskites [40,41], and cuprates (including Cu_2O and CuO) [33–36,42]. A recent theoretical study on rare-earth nickelates ($RNiO_3$), using comparable values of U_{dd} (=7 eV) and U_{pp} (=5 eV), showed that the metal-insulator transition in $RNiO_3$ arises from a novel charge order involving ligand holes [43]. While all the above-mentioned cuprate families show charge order [8–12], to date there is no report of charge order in the $HgBa_2Ca_2Cu_3O_{8+\delta}$(Hg1223) series, which shows the highest T_c (=134 K) at ambient pressure, [44] although a clear spin gap was reported early [13]. For single layer cuprates, it is known that the strength of correlations depends on the presence or absence of apical oxygens for the Cu site, with stronger effective correlations in hole-doped $La_{2-x}Sr_xCuO_4$ (LSCO) having apical oxygen, and weaker correlations in electron-doped $Nd_{2-x}Ce_xCuO_4$ (NCCO), having no apical oxygen [28,29]. Hg1223 has three Cu-O layers: the inner layer has no apical oxygen and the two outer layers have pyramidal CuO_5 coordination [45]. Using a single band Hubbard model, it was recently shown that the effective correlations are weakest in the Hg1223 system quite like the electron-doped cuprates [46]. Most importantly, in a three band model explicitly including U_{dd} and U_{pp}, it was shown that the static $U_{dd} = 7.0$ eV and $U_{pp} = 4.64$ eV for La_2CuO_4 [30]. Given these issues and a recent resurgence of interest in the Hg-based cuprates [45–49], we felt it important to quantify U_{dd} and U_{pp} for the optimally doped Hg1223. While the present work does not address the relationship of charge order with U_{dd} and U_{pp}, we hope our results help to understand the highest-T_c system, motivate studies for charge order in Hg1223, and clarify its link with U_{dd} and U_{pp} in general.

Photoemission spectroscopy (PES) has played a vital role in elucidating the electronic structure of high-T_c cuprates. High-resolution angle-resolved PES studies revealed the Fermi surfaces [26], a momentum-dependent pseudogap [50,51], a low energy kink in band dispersions

[16], and the highly intriguing Fermi arcs [52] whose origin is still under debate [53,54]. Core level PES in combination with model cluster calculations showed that $U_{dd} > \Delta$, the charge-transfer energy, and the low energy properties involve charge-transfer excitations in the Zaanen-Sawatzky-Allen scheme [55,56]. The properties of all the cuprate families originate in the CuO_4 plaquette common to their layered structure [26]. The strong hybridization of the Cu $3d$-O $2p$ states leads to the Zhang-Rice singlet (ZRS) as the lowest energy state [25]. For Bi2212 [57,58] and for LSCO [59,60], core level PES and spin-polarized resonant PES studies have established the ZRS state across the superconducting dome. Since the highest-T_c Hg1223 system also shows the superconducting dome behavior [45,61], it is important to identify and characterize the ZRS state in Hg1223.

We carry out x-ray absorption spectroscopy (XAS) and resonant PES across the O K edge and Cu L edge of optimally doped Hg1223. The samples were prepared by a high-pressure method and showed a superconducting $T_c = 134$ K (Fig. S1) [45]. The details of sample preparation, characterization, and spectroscopy measurements are described in Supplemental Material (SM) [62]. We also carry out off-resonant valence band (VB) PES at specific photon energies from 21.2–1200 eV to conclusively determine the O $2p$ and Cu $3d$ partial density of states (PDOS). Using the estimated U_{dd} and U_{pp}, we carry out model many-body Hamiltonian calculations for a Cu_2O_7 cluster with nonlocal screening [63,64] for the Cu $2p$ core level PES and Cu L-edge XAS spectra. The results show the importance of nonlocal screening in PES and XAS, and confirm the ZRS state as well as the estimated values of $U_{dd} = 6.5 \pm 1$ eV and $U_{pp} = 1.0 \pm 0.5$ eV. Thus, the highest-T_c cuprate exhibits an unexpectedly smaller U_{pp} compared to U_{dd}, i.e., coexistence of weakly correlated oxygen holes and strongly correlated d holes, which needs to be considered in theoretical models addressing the highest T_c in cuprates.

Figure 1 shows the VB PES of Hg1223 measured with ultraviolet (He I, $h\nu = 21.2$ eV) and soft x-ray ($h\nu \sim 524$, ~926 and 1200 eV) photons. The VB PES measured with $h\nu = 21.2$ eV shows a broad peak at 5 eV binding energy (BE) and a weak feature at 2.5 eV BE extending to the Fermi level, consistent with earlier work [65,66]. In spite of the very low intensity near E_F, the Hg1223 spectra show a Fermi step indicative of a metal. The near E_F Hg1223 spectrum measured with $h\nu = 21.2$ eV at $T = 120$ K is shown in the inset along with the Fermi step for gold and a Fermi-Dirac fit to the step. The superconducting gap at $T = 120$ K is too small to be measured with a resolution of ~40 meV. The feature at 5 eV BE is the O $2p$ band and the weak feature at 2.5 eV BE dominantly consists of the Cu $3d$ states, based on band structure calculations [67]. On increasing photon energies, the feature at 2.5 eV is relatively enhanced (the spectra are normalized at the 5 eV feature; see

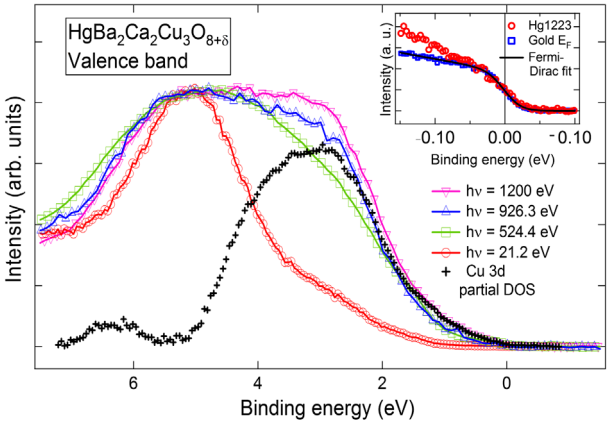

FIG. 1. Photon energy dependent valence band PES of $HgBa_2Ca_2Cu_3O_{8+\delta}$ (Hg1223) measured using $h\nu = 21.2$, 524.4, 926.3, and 1200 eV. The spectra are normalized at 5 eV BE. The experimental Cu $3d$ PDOS, obtained as a difference spectrum between $h\nu = 1200$ eV and $h\nu = 21.2$ eV spectra, is also plotted. The inset shows the Fermi step for Hg1223 and gold reference along with a fit to the Fermi-Dirac distribution convoluted with a Gaussian function. The He I ($h\nu = 21.2$ eV) spectrum is a laboratory measurement at $T = 120$ K and all other spectra are measured at $T = 20$ K using synchrotron radiation.

SM), confirming the assignment [33]. The core levels (Hg $4f$, Ba $3d$, Ca $2p$, and O $1s$) and wide BE range valence band spectrum showing also the Hg $5d$, Ba $5s$-$5p$, Ca $3p$, and O $2s$ shallow core levels measured with $h\nu =$ 1200 eV are discussed in Figs. S2 and S3 of SM [68].

In Fig. 2(a), we show the Cu L_3-edge XAS (inset shows the wide range L_3 and L_2 features), which consists of a main peak at ~931 eV photon energy (label **d**) and a weak but clear feature at ~933 eV (label **g**). The weak feature has been reported earlier but with much lower relative intensity [73]. We then carried out Cu $2p$-$3d$ resonant valence band PES at the photon energies labeled **a** − **j** and the spectra are correspondingly labeled and shown in Fig. 2(b). The off-resonance spectrum **a** is the same as the $h\nu = 926.3$ eV spectrum of Fig. 1. As we increase the photon energies from **a** to **d**, we see a dramatic ~190-times increase in the intensity of feature centered at 12.8 eV BE. This corresponds to the well-known giant resonance seen in cuprates [35]. On increasing the photon energy further, we see a shift of the resonance feature as it moves to higher binding energies, with the magnitude of the energy shift tracking the increase in photon energy. This identifies the resonance feature as the Cu L_3VV Auger state, with two final state holes (VV) in the valence band thus confirming its origin to be the Cu $3d$ correlation satellite. The intensity follows the XAS profile with a reduction for photon energies labeled **e** and **f**, then an increase at **g**, followed by a gradual reduction at higher energies.

In order to estimate U_{dd} and U_{pp}, we use the Cini-Sawatzky method [31–33,38,40]: determine the one-electron removal (single-hole) valence band Cu $3d$/O $2p$

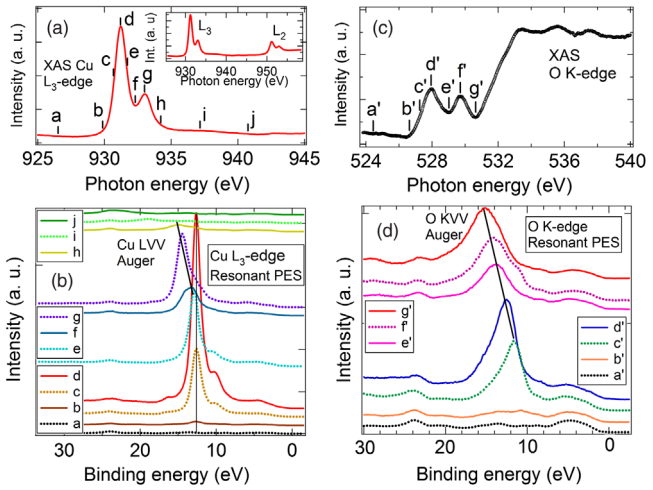

FIG. 2. (a) The Cu L_3-edge ($2p$-$3d$) XAS of Hg1223 measured at $T = 20$ K. The labels a–j indicate $h\nu$ used for measuring Cu $2p$-$3d$ resonant valence band PES of Hg1223 shown in panel (b). (b) Resonant PES showing the sharp peak at 12.6 eV BE obtained with $h\nu = 931.2$ eV [main peak in XAS; label **d** in panel (a)] is the $3d^8$ giant resonance feature. The thin black vertical line shows that the $3d^8$ resonance peak stays fixed at 12.8 eV BE up to $h\nu = 931.2$ eV and evolves into the Cu L_3VV Auger satellite for higher $h\nu$. (c) The O K edge ($1s$-$2p$) XAS of Hg1223 measured at $T = 20$ K. The labels $\mathbf{a}' - \mathbf{g}'$ mark the photon energies used for measuring the O $1s$-$2p$ resonant valence band PES shown in panel d. (d) The $2p^4$ resonance satellite arising due to on-site U_{pp} correlations gets enhanced but stays fixed up to a photon energy of 527.6 eV [label $\mathbf{c}'$ in panel (a)] and evolves into the O KVV Auger satellite for higher photon energies. All resonant PES spectra are normalized for incident photon flux and number of scans.

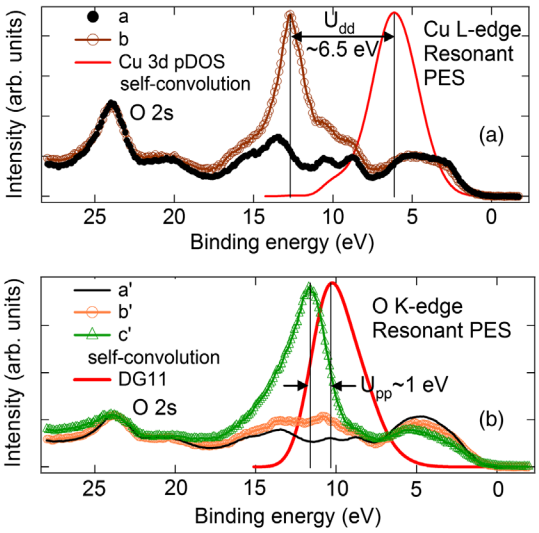

FIG. 3. (a) The Cu $2p$-$3d$ resonant PES spectra [labeled **a** and **b**, from Fig. 2(b)] measured at $T = 20$ K (normalized at the O $2s$ feature at ~24 eV BE) showing the resonantly enhanced correlation satellite at 12.8 eV compared with the self-convolution of Cu $3d$ PDOS shown in Fig. 1. The energy separation between the main peaks gives $U_{dd} = 6.5 \pm 0.5$ eV. (b) The O $1s$-$2p$ resonant PES spectra [labeled $\mathbf{a}' - \mathbf{c}'$, from Fig. 2(d)] measured at $T = 20$ K (normalized at the O $2s$ feature at ~24 eV BE) showing the resonantly enhanced correlation satellite at 11.6 eV BE compared with the self-convoluted O $2p$ PDOS. The energy separation between the main peaks gives $U_{pp} = 1.0 \pm 0.5$ eV.

PDOS, numerically evaluate the corresponding two-valence-hole energies as a self-convolution of the single-hole states, and then compare with the measured correlation satellite associated with the two-valence-hole (VV) Auger final state for estimating the site-specific Coulomb energies in compounds. We first identify the dominantly Cu 3d PDOS in the valence band. We do this by subtracting out the ultraviolet ($h\nu = 21.2$ eV) valence band spectrum (which consists mainly of the O $2p$ PDOS) from the soft x-ray ($h\nu = 1200$ eV) spectrum, both spectra normalized at 5 eV BE, as shown in Fig. 1. We carry out a self-convolution of the Cu $3d$ PDOS (Fig. S4; see SM for details) and compare it with the spectrum showing the resonantly enhanced Cu $3d$ correlation satellite that occurs at 12.8 eV BE (Fig. 3). The spectra labeled **a** and **b** are the same as shown in Fig. 2(b), but drawn on an expanded y scale and normalized to the O $2s$ core level peak at ~24 eV BE. The energy separation between the main peaks of the resonantly enhanced spectrum and the two-hole spectrum gives a measure of $U_{dd} = 6.5 \pm 0.5$ eV, consistent with earlier work on other cuprates [33–36].

Next, we carry out a similar analysis to determine U_{pp}, by measuring the O K-edge XAS [Fig. 2(c)] and O $1s$-$2p$ resonant valence band PES [Fig. 2(d)]. Labels $\mathbf{a}' - \mathbf{g}'$ in Fig. 2(c) mark photon energies used to measure the resonant PES spectra. The O $1s$-$2p$ resonant PES spectra shown in Fig. 2(d) thus identify the O KVV Auger feature originating in the O $2p$ correlation satellite, occurring at ~11.6 eV. In Fig. 3(b), we compare the self-convolution of the O $2p$ PDOS (Fig. S5) with the spectra $\mathbf{a}' - \mathbf{c}'$ showing the resonantly enhanced correlation satellite. The spectra labeled $\mathbf{a}' - \mathbf{c}'$ are the same as shown in Fig. 2(d), but plotted on an expanded y scale and normalized to the O $2s$ peak at ~24 eV BE. From the energy separation between the main peaks, we estimate $U_{pp} = 1.0 \pm 0.5$ eV. Such a low value of U_{pp} for $3d$ transition metal oxides, in general, and for hole-doped cuprates in particular, has not been reported to date.

It is well known that the Cu $2p$ core level PES is best explained by model many-body cluster calculations that go beyond a single CuO_4 plaquette by including nonlocal screening from a neighboring CuO_4 plaquette [63,64]. We have carried out such calculations for a Cu_2O_7 cluster [74] and compared the results with the experimentally measured Cu $2p$ PES. While nonlocal calculations for Cu L-edge XAS have shown an additional satellite feature [63], it has not been directly compared with experiment as most cuprates show only a single peak XAS spectrum that gets broadened with doping [35,75,76]. However, the Hg-based cuprates have shown a weak well-separated satellite feature [73]. In the present study, we also see a clear satellite that is

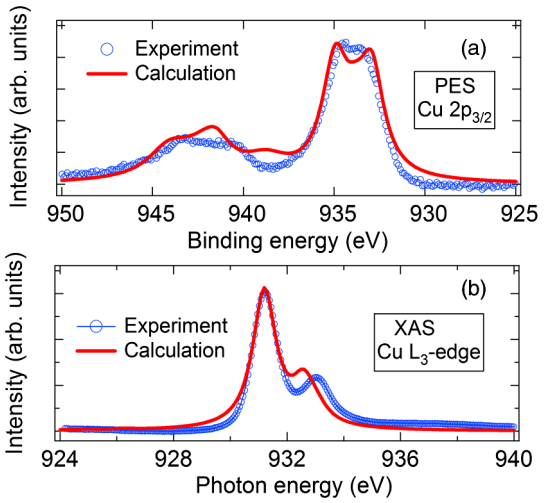

FIG. 4. (a) The Cu $2p_{3/2}$ PES of Hg1223 measured at $T = 20$ K compared with a Cu_2O_7 cluster calculation with nonlocal screening. (b) The Cu L_3-edge XAS of Hg1223 measured at $T = 20$ K compared with a Cu_2O_7 cluster calculation with nonlocal screening.

reproduced by calculations. The calculations (see SM for details) were carried out for the simplest case with three holes in the Cu_2O_7 cluster, corresponding to 50% hole doping.

Fig. 4(a) shows the Cu $2p_{3/2}$ experimental core level PES spectrum plotted with the calculated spectrum. The experimental data show a main peak consisting of two features at 933.4 and 934.5 eV, and broad weak intensity satellite structures between ~939 and ~946 eV. The calculated spectrum was obtained using $\Delta = 1.3$ eV, where Δ is the charge-transfer energy, the O $2p-$Cu $3d$ overlap integral $t_{pd} = 0.45$ eV, the O $2p-$O $2p$ overlap integral $t_{pp} = 0.3$ eV, $U_{dd} = 6.5$ eV, $U_{pp} = 1.0$ eV, and the Coulomb interaction due to the core hole $U_{dc} = 8.5$ eV. While the calculations reproduce all the features of the experimental data but with small discrepancies for the satellite features, we use the above parameters as they give the best fit to the Cu $2p$ PES and L-edge XAS spectra simultaneously. We checked that the well-screened feature at 933.4 eV in the Cu $2p_{3/2}$ main peak (the lowest BE feature) is dominated by the Cu1 $\underline{c}d^{10}\underline{L}^1$: Cu2 $d^9\underline{L}^1$ configuration (the prefix Cu1 and Cu2 identify the two Cu sites and the core hole $\underline{c}$ is created on the Cu1 site; see Fig. S6 in SM). Thus, the well-screened feature involves nonlocal screening from the Cu2-site CuO_4 plaquette, leading to an effective ZRS state consistent with earlier work [63,64]. The feature at 934.5 eV in the main peak is attributed to local screening from the Cu1-site plaquette as it is dominated by Cu1 $\underline{c}d^9\underline{L}^1$: Cu2 d^9, and Cu1 $\underline{c}d^{10}\underline{L}^2$: Cu2 d^9 states, with admixture from Cu1 $\underline{c}d^{10}\underline{L}^2$: Cu2 $d^{10}\underline{L}^1$. The satellite features are dominated by ionic configurations on the Cu1 site, namely, Cu1 $\underline{c}d^9$: Cu2 $\underline{c}d^9\underline{L}^1$ and Cu1 $\underline{c}d^9$: Cu2 $\underline{c}d^{10}\underline{L}^2$ with admixture from $\underline{c}d^9\underline{L}^1$: Cu2 d^9 and $\underline{c}d^{10}\underline{L}^1$: Cu2 d^8 configurations. We confirmed the validity of the parameters by varying U_{dd} and U_{pp} values, as shown in Figs. S7 and S8, keeping all other parameters fixed. The calculations indicate deviations from experimental data if $U_{dd} < 4$ eV or $U_{pp} \geq 3$ eV (see SM for details).

Similarly, Fig. 4(b) shows the Cu L_3 XAS spectrum compared to calculations carried out with the same parameters as for the Cu $2p$ core level PES discussed above. The main peak in the Cu L_3 XAS spectrum at ~931 eV is dominated by the $\underline{c}d^{9+1}\underline{L}^1$: Cu2 $d^{10}\underline{L}^1$ state involving nonlocal screening from the Cu2 site, with admixture from the $\underline{c}d^{9+1}\underline{L}^1$: Cu2 d^9 state. The satellite feature at ~933 eV is dominated by the $\underline{c}d^{9+1}\underline{L}^1$: Cu2 d^9 state with admixture from $\underline{c}d^{8+1}$: Cu2 $d^{10}\underline{L}^1$. The results confirm a large U_{dd} coexisting with a small U_{pp} in the highest-T_c Hg1223 cuprate, and indicate an electronic inhomogeneity on the length scale of a CuO_4 plaquette.

Our results indicate the necessity of distinguishing between U_{dd} and U_{pp}, which originates from dynamical screening effects at the Cu and O site in a three band model [30]. It was shown by Werner *et al.* that the static $U_{dd} = 7.0$ eV, and is larger than $U_{pp} = 4.64$ eV, for La_2CuO_4 [30]. The authors also discussed that the frequency dependent local self-energy is larger for the Cu site with four nearest neighbor oxygens, and smaller for the O site with two nearest neighbor Cu atoms. For the single band Hubbard model, a very recent extension showed that U_{dd} is reduced for the Hg-based cuprates, as it is proportional to the inverse of the bond distance between apical oxygen and copper atoms [46]. Finally, since the charge carriers in the hole-doped cuprates have large O $2p$ hole character, coexistence of a small U_{pp} and large U_{dd} suggests pairing would be favored for the weakly correlated oxygen holes in the highest-T_c Hg1223 cuprate.

In conclusion, resonant valence band PES across the O K edge and Cu L edge identifies correlation satellites due to two-hole final states in Hg1223. Analyses using the measured O $2p$ and Cu $3d$ partial DOS show that on-site Coulomb energy for the O site ($U_{pp} = 1.0 \pm 0.5$ eV) is much smaller than that for the Cu site ($U_{dd} = 6.5 \pm 0.5$ eV). Cu_2O_7-cluster calculations with nonlocal screening for the Cu $2p$ core level PES and Cu L-edge XAS spectra confirm the U_{dd} and U_{pp} values, and provide evidence for the Zhang-Rice singlet state in optimally doped Hg1223. In contrast to known results of $U_{pp} \sim U_{dd}$ for other hole-doped cuprates as well as $3d$-transition metal oxides in general, the present results indicate weakly correlated oxygen holes in the highest-T_c cuprate Hg1223.

A. C. thanks the Institut Jean Lamour, Université de Lorraine for hospitality and financial support during the course of this work. The synchrotron radiation experiments were performed at BL17SU, SPring-8, with the approval of RIKEN (Grant No. 20140019).

[1] J. G. Bednorz and K. A. Mueller, Z. fur Physik B **64**, 189 (1986).
[2] J. Zaanen and O. Gunnarsson, Phys. Rev. B **40**, 7391(R) (1989).
[3] K. Machida, Physica (Amsterdam) **158C**, 192 (1989); M. Kato, K. Machida, H. Nakanishi, and M. Fujita, J. Phys. Soc. Jpn. **59**, 1047 (1990).
[4] S.-W. Cheong, G. Aeppli, T. E. Mason, H. Mook, S. M. Hayden, P. C. Canfield, Z. Fisk, K. N. Clausen, and J. L. Martinez, Phys. Rev. Lett. **67**, 1791 (1991).
[5] J. M. Tranquada, B. J. Sternlieb, J. D. Axe, Y. Nakamura, and S. Uchida, Nature (London) **375**, 561 (1995).
[6] M. I. Salkola, V. J. Emery, and S. A. Kivelson, Phys. Rev. Lett. **77**, 155 (1996).
[7] T. Wu, H. Mayaffre, S. Kramer, M. Horvatic, C. Berthier, W. N. Hardy, R. Liang, D. A. Bonn, and M.-H. Julien, Nature (London) **477**, 191 (2011).
[8] G. Ghiringhelli, M. Le Tacon, M. Minola, S. Blanco-Canosa, C. Mazzoli, N. B. Brookes, G. M. De Luca, A. Frano, D. G. Hawthorn, F. He, T. Loew, M. Moretti Sala, D. C. Peets, M. Salluzzo, E. Schierle, R. Sutarto, G. A. Sawatzky, E. Weschke, B. Keimer, and L. Braicovich, Science **337**, 821 (2012).
[9] J. Chang, E. Blackburn, A. T. Holmes, N. B. Christensen, J. Larsen, J. Mesot, R. Liang, D. A. Bonn, W. N. Hardy, A. Watenphul, M. v. Zimmermann, E. M. Forgan, and S. M. Hayden, Nat. Phys. **8**, 871 (2012).
[10] M. Le Tacon, A. Bosak, S. M. Souliou, G. Dellea, T. Loew, R. Heid, K.-P. Bohnen, G. Ghiringhelli, M. Krisch, and B. Keimer, Nat. Phys. **10**, 52 (2014).
[11] W. Tabis, Y. Li, M. Le Tacon, L. Braicovich, A. Kreyssig, M. Minola, G. Dellea, E. Weschke, M. J. Veit, M. Ramazanoglu, A. I. Goldman, T. Schmitt, G. Ghiringhelli, N. Barisic, M. K. Chan, C. J. Dorow, G. Yu, X. Zhao, B. Keimer, and M. Greven, Nat. Commun. **5**, 5875 (2014).
[12] S. Gerber, H. Jang, H. Nojiri, S. Matsuzawa, H. Yasumura, D. A. Bonn, R. Liang, W. N. Hardy, Z. Islam, A. Mehta, S. Song, M. Sikorski, D. Stefanescu, Y. Feng, S. A. Kivelson, T. P. Devereaux, Z.-X. Shen, C.-C. Kao, W.-S. Lee, D. Zhu, and J.-S. Lee, Science **350**, 949 (2015).
[13] M.-H. Julien, P. Carretta, M. Horvatic, C. Berthier, Y. Berthier, P. Segransan, A. Carrington, and D. Colson, Phys. Rev. Lett. **76**, 4238 (1996).
[14] W. S. Lee, J. J. Lee, E. A. Nowadnick, S. Gerber, W. Tabis, S. W. Huang, V. N. Strocov, E. M. Motoyama, G. Yu, B. Moritz, H. Y. Huang, R. P. Wang, Y. B. Huang, W. B. Wu, C. T. Chen, D. J. Huang, M. Greven, T. Schmitt, Z. X. Shen, and T. P. Devereaux, Nat. Phys. **10**, 883 (2014).
[15] M. K. Chan, C. J. Dorow, L. Mangin-Thro, Y. Tang, Y. Ge, M. J. Veit, G. Yu, X. Zhao, A. D. Christianson, J. T. Park, Y. Sidis, P. Steffens, D. L. Abernathy, P. Bourges, and M. Greven, Nat. Commun. **7**, 10819 (2016).
[16] A. Lanzara, P. V. Bogdanov, X. J. Zhou, S. A. Kellar, D. L. Feng, E. D. Lu, T. Yoshida, H. Eisaki, A. Fujimori, K. Kishio, J.-I. Shimoyama, T. Noda, S. Uchida, Z. Hussain, and Z.-X. Shen, Nature (London) **412**, 510 (2001).
[17] B. Keimer, S. A. Kivelson, M. R. Norman, S. Uchida, and J. Zaanen, Nature (London) **518**, 179 (2015).
[18] T. Valla, A. V. Fedorov, P. D. Johnson, B. O. Wells, S. L. Hulbert, Q. Li, G. D. Gu, and N. Koshizuka, Science **285**, 2110 (1999).
[19] I. Hetel, T. R. Lemberger, and M. Randeria, Nat. Phys. **3**, 700 (2007).
[20] K. B. Efetov, H. Meier, and C. Pépin, Nat. Phys. **9**, 442 (2013).
[21] Th. Jacobs, Y. Simsek, Y. Koval, P. Muller, and V. M. Krasnov, Phys. Rev. Lett. **116**, 067001 (2016).
[22] S. Badoux, W. Tabis, F. Laliberte, G. Grissonnanche, B. Vignolle, D. Vignolles, J. Beard, D. A. Bonn, W. N. Hardy, R. Liang, N. Doiron-Leyraud, Louis Taillefer, and Cyril Proust, Nature (London) **531**, 210 (2016).
[23] V. J. Emery, Phys. Rev. Lett. **58**, 2794 (1987).
[24] C. M. Varma, S. Schmitt-Rink, and E. Abrahams, Solid State Commun. **62**, 681 (1987).
[25] F. C. Zhang and T. M. Rice, Phys. Rev. B **37**, 3759 (1988).
[26] A. Damascelli, Z. Hussain, and Z.-X. Shen, Rev. Mod. Phys. **75**, 473 (2003).
[27] P. A. Lee, N. Nagaosa, and X. -G Wen, Rev. Mod. Phys. **78**, 17 (2006).
[28] H. Das and T. Saha-Dasgupta, Phys. Rev. B **79**, 134522 (2009).
[29] C. Weber, K. Haule, and G. Kotliar, Nat. Phys. **6**, 574 (2010); Phys. Rev. B **82**, 125107 (2010).
[30] P. Werner, R. Sakuma, F. Nilsson, and F. Aryasetiawan, Phys. Rev. B **91**, 125142 (2015).
[31] M. Cini, Solid State Commun. **20**, 605 (1976); **24**, 681 (1977); Phys. Rev. B **17**, 2788 (1978).
[32] G. A. Sawatzky, Phys. Rev. Lett. **39**, 504 (1977).
[33] D. van der Marel, J. van Elp, G. A. Sawatzky, and D. Heitmann, Phys. Rev. B **37**, 5136 (1988).
[34] A. Balzarotti, M. De Crescenzi, N. Motta, F. Patella, and A. Sgarlata, Phys. Rev. B **38**, 6461 (1988).
[35] L. H. Tjeng, C. T. Chen, and S.-W. Cheong, Phys. Rev. B **45**, 8205 (1992).
[36] R. Bar-Deroma, J. Felsteiner, R. Brener, J. Ashkenazi, and D. van der Marel, Phys. Rev. B **45**, 2361 (1992).
[37] Y. Ishida, R. Eguchi, M. Matsunami, K. Horiba, M. Taguchi, A. Chainani, Y. Senba, H. Ohashi, H. Ohta, and S. Shin, Phys. Rev. Lett. **100**, 056401 (2008).
[38] G. A. Sawatzky and D. Post, Phys. Rev. B **20**, 1546 (1979).
[39] J.-H. Park, Ph.D. thesis, University of Michigan, 1994.
[40] A. Chainani, M. Mathew, and D. D. Sarma, Phys. Rev. B **46**, 9976 (1992); **47**, 15397 (1993); A. Chainani, M. Mathew, and D. D. Sarma, Phys. Rev. B **48**, 14818 (1993); A. Chainani, Ph.D. thesis, Indian Institute of Science, 1993.
[41] D. D. Sarma and A. Chainani, J. Solid State Chem. **111**, 208 (1994).
[42] J. Ghijsen, L. H. Tjeng, J. van Elp, H. Eskes, J. Westerink, G. A. Sawatzky, and M. T. Czyzyk, Phys. Rev. B **38**, 11322 (1988).
[43] S. Johnston, A. Mukherjee, I. Elfimov, M. Berciu, and G. A. Sawatzky, Phys. Rev. Lett. **112**, 106404 (2014).
[44] A. Schilling, M. Cantoni, J. D. Guo, and H. R. Ott, Nature (London) **363**, 56 (1993).
[45] A. Yamamoto, N. Takeshita, C. Terakura, and Y. Tokura, Nat. Commun. **6**, 8990 (2015).
[46] S.-W. Jang, H. Sakakibara, H. Kino, T. Kotani, K. Kuroki, and M.-J Han, Sci. Rep. **6**, 33397 (2016).
[47] J. P. Hinton, E. Thewalt, Z. Alpichshev, F. Mahmood, J. D. Koralek, M. K. Chan, M. J. Veit, C. J. Dorow, N. Barisic, A. F. Kemper, D. A. Bonn, W. N. Hardy, R. Liang,

N. Gedik, M. Greven, A. Lanzara, and J. Orenstein, arXiv:1601.05224.
[48] B. Loret, S. Sakai, Y. Gallais, M. Cazayous, M.-A. Measson, A. Forget, D. Colson, M. Civelli, and A. Sacuto, Phys. Rev. Lett. **116**, 197001 (2016).
[49] M. Izquierdo, D. C. Freitas, D. Colson, G. Garbarino, A. Forget, S. Megtert, H. Raffy, R. Comes, J.-P. Itie, S. Ravy, P. Fertey, and M. Nunez-Regueiro, arXiv:1510.03750.
[50] D. S. Marshall, D. S. Dessau, A. G. Loeser, C.-H. Park, A. Y. Matsuura, J. N. Eckstein, I. Bozovic, P. Fournier, A. Kapitulnik, W. E. Spicer, and Z.-X. Shen, Phys. Rev. Lett. **76**, 4841 (1996).
[51] H. Ding, T. Yokoya, J. C. Campuzano, T. Takahashi, M. Randeria, M. R. Norman, T. Mochiku, K. Kadowaki, and J. Giapintzakis, Nature (London) **382**, 51 (1996).
[52] M. R. Norman, H. Ding, M. Randeria, J. C. Campuzano, T. Yokoya, T. Takeuchi, T. Takahashi, T. Mochiku, K. Kadowaki, P. Guptasarma, and D. G. Hinks, Nature (London) **392**, 157 (1998).
[53] J. Meng, G. Liu, W. Zhang, L. Zhao, H. Liu, X. Jia, D. Mu, S. Liu, X. Dong, J. Zhang, W. Lu, G. Wang, Y. Zhou, Y. Zhu, X. Wang, Z. Xu, C. Chen, and X. J. Zhou, Nature (London) **462**, 335 (2009).
[54] P. D. C. King, J. A. Rosen, W. Meevasana, A. Tamai, E. Rozbicki, R. Comin, G. Levy, D. Fournier, Y. Yoshida, H. Eisaki, K. M. Shen, N. J. C. Ingle, A. Damascelli, and F. Baumberger, Phys. Rev. Lett. **106**, 127005 (2011).
[55] A. Fujimori, E. Takayama-Muromachi, Y. Uchida, and B. Okai, Phys. Rev. B **35**, 8814(R) (1987).
[56] Z.-X. Shen, J. W. Allen, J. J. Yeh, J.-S. Kang, W. Ellis, W. Spicer, I. Lindau, M. B. Maple, Y. D. Dalichaouch, M. S. Torikachvili, J. Z. Sun, and T. H. Geballe, Phys. Rev. B **36**, 8414 (1987).
[57] M. A. van Veenendaal, G. A. Sawatzky, and W. A. Groen, Phys. Rev. B **49**, 1407 (1994).
[58] N. B. Brookes, G. Ghiringhelli, O. Tjernberg, L. H. Tjeng, T. Mizokawa, T. W. Li, and A. A. Menovsky, Phys. Rev. Lett. **87**, 237003 (2001).
[59] M. Taguchi, A. Chainani, K. Horiba, Y. Takata, M. Yabashi, K. Tamasaku, Y. Nishino, D. Miwa, T. Ishikawa, T. Takeuchi, K. Yamamoto, M. Matsunami, S. Shin, T. Yokoya, E. Ikenaga, K. Kobayashi, T. Mochiku, K. Hirata, J. Hori, K. Ishii, F. Nakamura, and T. Suzuki, Phys. Rev. Lett. **95**, 177002 (2005).
[60] N. B. Brookes, G. Ghiringhelli, A.-M. Charvet, A. Fujimori, T. Kakeshita, H. Eisaki, S. Uchida, and T. Mizokawa, Phys. Rev. Lett. **115**, 027002 (2015).
[61] A. Fukuoka, A. Tokiwa-Yamamoto, M. Itoh, R. Usami, S. Adachi, and K. Tanabe, Phys. Rev. B **55**, 6612 (1997).
[62] Material synthesis and characaterization, experimental methods, supporting spectroscopy, and model many-body Cu_2O_7-cluster calculation methods and results are detailed in Supplemental Material.
[63] M. A. van Veenendaal, H. Eskes, and G. A. Sawatzky, Phys. Rev. B **47**, 11462 (1993); M. A. van Veenendaal and G. A. Sawatzky, Phys. Rev. B **49**, 3473 (1994).
[64] K. Okada and A. Kotani, Phys. Rev. B **52**, 4794 (1995).
[65] P. Almeras, T. DellfOrto, C. Coluzza, J. Almeida, G. Margaritondo, Y. Y. Xue, R. L. Meng, and C. W. Chu, J. Appl. Phys. **76**, 1100 (1994).
[66] R. P. Vasquez, M. Rupp, A. Gupta, and C. C. Tsuei, Phys. Rev. B **51**, 15657(R) (1995).
[67] D. J. Singh, Physica (Amsterdam) **212C**, 228 (1993); C. O. Rodriguez, N. E. Christensen, and E. L. Peltzer y Blanca, Physica (Amsterdam) **216C**, 12 (1993).
[68] See Supplemental Material http://link.aps.org/supplemental/10.1103/PhysRevLett.119.057001 for detailed characterization of the core level and valence band spectra, which includes Refs. [69–72].
[69] J. F. Moulder, W. F. Stickle, P. E. Sobol, and K. D. Bomben, *Handbook of X-Ray Photoelectron Spectroscopy* (Physical Electronics, Eden Prairie, MN, 1995).
[70] C. S. Gopinath, N. H. Hur, and S. Subramanian, Phys. Rev. B **52**, R9879 (1995).
[71] F. Parmigiani and L. Sangaletti, J. Electron Spectrosc. Relat. Phenom. **98–99**, 287 (1999).
[72] J. J. Yeh, I. Lindau, At. Data Nucl. Data Tables **32**, 1 (1985).
[73] E. Pellegrin, J. Fink, C. T. Chen, Q. Xiong, Q. M. Lin, and C. W. Chu, Phys. Rev. B **53**, 2767 (1996).
[74] A. Chainani and D. Malterre (to be published).
[75] C. T. Chen, L. H. Tjeng, J. Kwo, H. L. Kao, P. Rudolf, F. Sette, and R. M. Fleming, Phys. Rev. Lett. **68**, 2543 (1992).
[76] N. Nucker, E. Pellegrin, P. Schweiss, J. Fink, S. L. Molodtsov, C. T. Simmons, G. Kaindl, W. Frentrup, A. Erb, and G. Muller-Vogt, Phys. Rev. B **51**, 8529 (1995).